UNIVERSITÄT AUGSBURG
Universitätsbibliothek

OPEN ACCESS
OPUS AUGSBURG

A Copula-XAI framework for assessing compound typhoon disaster-chain risks and driving mechanisms in coastal mountainous cities: evidence from Fujian, China

Xiaoliu Yang, Xiaochen Qin, Miaomiao Ma, Jiewen You, Ying Chen, Laiyin Zhu, Jianhui Wei, Lu Gao, Harald Kunstmann

Angaben zur Veröffentlichung / Publication details:

Yang, Xiaoliu, Xiaochen Qin, Miaomiao Ma, Jiewen You, Ying Chen, Laiyin Zhu, Jianhui Wei, Lu Gao, and Harald Kunstmann. 2026. "A Copula-XAI framework for assessing compound typhoon disaster-chain risks and driving mechanisms in coastal mountainous cities: evidence from Fujian, China." *Journal of Hydrology: Regional Studies* 64: 103284. https://doi.org/10.1016/j.ejrh.2026.103284.

Nutzungsbedingungen / Terms of use: **CC BY-NC-ND 4.0**

Dieses Dokument wird unter folgenden Bedingungen zur Verfügung gestellt: / This document is made available under these conditions:
CC-BY-NC-ND 4.0: Creative Commons: Namensnennung - Nicht kommerziell - Keine Bearbeitung
Weitere Informationen finden Sie unter: / For more information see:
https://creativecommons.org/licenses/by-nc-nd/4.0/deed.de

Journal of Hydrology: Regional Studies 64 (2026) 103284

Contents lists available at ScienceDirect

Journal of Hydrology: Regional Studies

journal homepage: www.elsevier.com/locate/ejrh

A Copula-XAI framework for assessing compound typhoon disaster-chain risks and driving mechanisms in coastal mountainous cities: Evidence from Fujian, China

Xiaoliu Yang [a], Xiaochen Qin [b], Miaomiao Ma [c], Jiewen You [a,d,e], Ying Chen [a,d,e], Laiyin Zhu [f], Jianhui Wei [g], Lu Gao [a,d,e,*], Harald Kunstmann [g,h,i]

[a] School of Geographical Sciences, Fujian Normal University, Fuzhou 350117, China
[b] Faculty of Geographical Science, Beijing Normal University, Beijing 100875, China
[c] China Institute of Water Resources and Hydropower Research, Beijing 100038, China
[d] Key Laboratory for Humid Subtropical Eco-Geographical Processes of the Ministry of Education, Fujian Normal University, Fuzhou 350117, China
[e] Fujian Provincial Engineering Research Center for Monitoring and Accessing Terrestrial Disasters, Fujian Normal University, Fuzhou 350117, China
[f] School of Environment, Geography, and Sustainability, Western Michigan University, Kalamazoo, MI 49008, USA
[g] Institute of Meteorology and Climate Research (IMKIFU), Karlsruhe Institute of Technology, Campus Alpin, Garmisch-Partenkirchen 82467, Germany
[h] Institute of Geography, University of Augsburg, Augsburg 86159, Germany
[i] Centre for Climate Resilience, University of Augsburg, Augsburg 86159, Germany

ARTICLE INFO

Keywords:
Typhoon disaster chains
Single disaster chains
Compound disaster chains
Copula-based joint probability
Explainable machine learning

ABSTRACT

Study region: Fujian Province, China.
Study focus: To address the limited quantitative understanding of compound disaster chain risks in highly urbanized mountainous coastal regions, this study develops an integrated framework combining a Copula-based joint probability model with explainable machine learning (XGBoost–SHAP). Using Fujian Province as a case study, we identify high-risk areas, quantify exposure inequality, and analyze key driving factors, nonlinear thresholds, and transition mechanisms across typical typhoon disaster chains.
New insights for the region: High-risk areas of typhoon disaster chains in Fujian Province show a clear spatial contrast, with single disaster chains being widely distributed and compound disaster chains strongly clustered. Although compound-chain high-risk areas account for only 0.8 % of the provincial area, they concentrate 12.6 % of the population and 14.1 % of economic activity. Correspondingly, population and GDP exposure lift values reach 16.3 and 18.2, respectively, which are substantially higher than those of single disaster chains, indicating pronounced exposure inequality. Overall, typhoon disaster chain risks follow a "natural triggering–social amplification" pathway and exhibit nonlinear threshold behavior. Transitions from single to compound disaster chains are governed by two dominant pathways: socioeconomic-driven and naturally driven transitions. These findings support fine-scale identification and differentiated management of compound disaster chain risks in mountainous coastal cities.

* Corresponding author at: School of Geographical Sciences, Fujian Normal University, Fuzhou 350117, China.
E-mail address: l.gao@foxmail.com (L. Gao).

https://doi.org/10.1016/j.ejrh.2026.103284
Received 29 November 2025; Received in revised form 19 January 2026; Accepted 20 February 2026
Available online 24 February 2026
2214-5818/© 2026 The Author(s). Published by Elsevier B.V. This is an open access article under the CC BY-NC-ND license (http://creativecommons.org/licenses/by-nc-nd/4.0/).

1. Introduction

Tropical cyclones (TCs) are intense tropical storms that form over the western North Pacific and the South China Sea, with maximum sustained wind speeds exceeding 32.7 m/s^{-1} (Beaufort scale $\geq$ 12). They represent the most frequent and destructive natural hazards affecting coastal southeastern China (Xi et al., 2023; Tran et al., 2022). TC events are typically accompanied by strong winds and persistent heavy rainfall, which can rapidly trigger multiple secondary hazards, including river flooding, urban waterlogging, landslides, and storm surges. Through temporal succession or spatial interaction, these hazards often form complex typhoon disaster chains (Zhu et al., 2023; Peduzzi et al., 2012). Under the combined effects of climate warming and rapid urbanization, coastal regions are increasingly exposed to concurrent or successive extreme rainfall, strong winds, and storm surges during TC events. The co-occurrence of multiple hazards substantially amplifies impacts on buildings, infrastructure, and socio-economic systems (Dottori et al., 2022; Gori et al., 2022; Wahl et al., 2015; Bevacqua et al., 2020). Compared with single extreme events, compound climate and weather extremes involve multiple interacting drivers or hazard processes and often exhibit strong nonlinear amplification effects (Mazdiyasni and AghaKouchak, 2015; Zscheischler et al., 2018; Raymond et al., 2020; Messori et al., 2021). In the context of TCs, the simultaneous or sequential occurrence of strong winds and heavy rainfall facilitates coupling among floods, urban waterlogging, landslides, and storm surges, leading to highly destructive compound typhoon disaster chains. These processes weaken emergency response capacity across scales and reduce the resilience of both natural and human systems, resulting in pronounced loss amplification effects (AghaKouchak et al., 2018; Otto et al., 2020). Consequently, developing a systematic understanding of compound typhoon disaster chains and their interacting hazard processes has become a key scientific challenge for improving regional disaster risk identification and management.

In recent years, the compound effects of typhoon disaster chains have received increasing attention. Previous studies indicate that TCs often simultaneously generate strong winds, intense rainfall, and storm surges, which significantly reduce the resistance of coastal infrastructure systems (Mitsova et al., 2018). Research in the United States provides a representative example of this evolving understanding. Early studies mainly focused on single extreme rainfall events, whereas catastrophic events such as Hurricanes Harvey and Florence prompted systematic investigations of the combined effects of rainfall, wind, and storm surge. These hazard drivers can act concurrently or sequentially. For example, rainfall combined with storm surge can trigger compound flooding and lead to more severe cascading damages (Gori et al., 2020, 2022). Such impacts are particularly evident in low-lying and densely populated estuarine cities along the Atlantic and Gulf coasts of the United States (Feng et al., 2022; Bates et al., 2021; Hallegatte et al., 2013). Long-term assessments further show that, during 1930–2015, each TC event along the U.S. coast caused an average of 7000–11,000 excess deaths, with disproportionately higher risks for vulnerable populations (Young and Hsiang, 2024). Meanwhile, the spatiotemporal overlap between extreme rainfall and storm surge in coastal regions continues to intensify and is reshaping global coastal flood risk under climate change (Lin et al., 2012; Marsooli et al., 2019). Similar compound-risk patterns have also been identified in other regions, including wind–rainfall compound hazard hotspots along the eastern coast and adjacent inland areas of India (Ranjan and Karmakar, 2024), as well as multiple highly urbanized coastal regions in China (Wang and Peng, et al., 2024). Collectively, these studies demonstrate that TC-induced compound disaster chains have become a common global challenge for coastal regions and pose disproportionate risks to vulnerable populations.

Coastal southeastern China is characterized by highly fragmented terrain and dense concentrations of population and economic activity. This region combines high hazard susceptibility with high exposure and represents a typical setting where typhoon disaster chains are easily formed and amplified, resulting in diverse disaster chain types and complex impact processes (Chen et al., 2007; Tang et al., 2023; Wang and Nan, et al., 2024). Fujian Province is particularly representative of these conditions. Located in a TC-prone zone along China's southeastern coast, the province is affected by approximately four to five TCs each year. Its predominantly mountainous topography, together with a spatial configuration of coastal basins, intermontane basins, and river valleys, leads to strong concentrations of population and assets in low-elevation areas. This configuration substantially increases the likelihood that intense rainfall and strong winds locally trigger urban waterlogging, river flooding, landslides, and storm surges, and promotes the formation and amplification of complex typhoon disaster chains (Yang and Qin, et al., 2024; Zscheischler et al., 2818, 2020; Yang et al., 2025). Similar combinations of complex terrain, high exposure, and strong TC disturbances are widespread along the southeastern coast of China and across many coastal regions in East and Southeast Asia (Chen et al., 2024; Wang and Nan, et al., 2024; Tang et al., 2023). Therefore, Fujian Province provides an ideal case for investigating compound typhoon disaster chains, offering important insights into cascading hazard processes and risk amplification mechanisms, while supporting the development of transferable regional risk assessment approaches.

Despite growing recognition of the compound nature of typhoon disaster chains, substantial gaps remain in hazard-chain characterization, mechanism analysis, and quantitative risk assessment. Existing studies have mainly focused on TC-induced compound flooding, such as river flooding combined with storm surge, urban waterlogging combined with river flooding, or river–coastal compound floods (Do and Kuleshov, 2023; Malakar et al., 2021; Lockwood et al., 2024; Deb et al., 2023). Some studies have also examined the combined effects of heavy rainfall and strong winds (Ravi et al., 2024). However, in mountainous and hilly cities, complex terrain conditions often lead to the concurrent or cascading interaction of river flooding, urban waterlogging, and landslides, yet these multi-hazard-chain processes and their spatial patterns remain poorly quantified. Moreover, existing assessment approaches mainly emphasize hazard intensity and frequently rely on two- or three-dimensional hydrodynamic models to simulate physical variables such as flood depth and duration (Grimley et al., 2024; Chen et al., 2024). Although effective for process simulation, these models require substantial computational resources and high-quality input data, which limits their applicability for large-scale, multi-scenario, and long-term analyses. In addition, they often insufficiently account for socio-economic exposure, vulnerability, and disaster mitigation capacity, potentially leading to systematic underestimation of compound risk. Recent studies have attempted

to apply deep learning and machine learning techniques for flood risk prediction (Peng et al., 2025; Dey and Haque, et al., 2024). However, for typhoon disaster-chain research, large differences in disaster loss statistics across countries, together with the scarcity of multi-hazard-chain samples and limited data accessibility, strongly constrain the applicability of data-intensive methods for compound risk quantification. From a disaster risk management perspective, systematically identifying the spatial distribution of high-risk areas, hazard-chain combinations, types, and associated exposure at the regional scale is essential for enabling targeted disaster prevention and differentiated intervention strategies (Haque et al., 2022; Dey and Shao, et al., 2024). Such information supports local threat identification, high-risk mapping, resource prioritization, and decision-making by different authorities during both pre-disaster planning and emergency response phases (VanDyke et al., 2021; Turner et al., 2003). Nevertheless, comprehensive studies addressing the risks, exposure patterns, and formation mechanisms of compound typhoon disaster chains remain limited, particularly in coastal southeastern China, where complex terrain coincides with high population density.

To address these gaps, this study focuses on Fujian Province and develops an integrated analytical framework that combines a multidimensional indicator system, Copula-based joint probability modeling, and explainable machine learning techniques. The Copula model is used to characterize nonlinear dependence structures and joint extreme occurrence probabilities among multiple hazards, while explainable machine learning is applied to identify key driving factors and their threshold effects across different disaster chain types. This framework balances statistical robustness with mechanistic interpretability and is well suited for compound disaster chain analysis in regions with complex terrain and high exposure. Compared with single-hazard or purely physics-based approaches commonly adopted in previous studies, this framework provides an integrated probabilistic and data-driven structure that explicitly accounts for hazard dependence, exposure, and interpretable drivers. Within this framework, a 30 arc-second (approximately 1 km) grid is adopted as the basic assessment unit to systematically identify the spatial combination patterns, types, and exposure characteristics of typhoon disaster chains. The study further analyzes dominant driving factors and quantifies the key drivers and critical thresholds associated with transitions from single to compound disaster chains. The main objectives of this study are to: (1) identify spatial patterns and types of typhoon disaster chains at a fine grid scale and reveal the distribution of high-risk areas and exposure inequality; (2) quantify key driving factors and their threshold dependencies for different disaster-chain types, clarifying the relative contributions of natural and social factors; and (3) characterize the critical controls and transition conditions from single to compound disaster chains to improve understanding of compound risk amplification mechanisms.

2. Methods

2.1. Study Area

Fujian Province (23°33′-28°20′N, 115°50′-120°40′E) has a land area of approximately 124,000 km^2 and a coastline of 3324 km. The terrain is dominated by mountains and hills, which account for about 89 % of the province's total area (Chen et al., 2007). Fujian lies in

Table 1
Data sets and variables used in this study.

Type	Dataset	Resolution	Period	Source
Foundational geospatial data	Administrative division data	N/A (vector data)	2024	Tianditu (http://lbs.tianditu.gov.cn/home.html)
	Coastline data	N/A (vector data)	2020	A Global Self-consistent, Hierarchical, High-resolution Geography (GSHHG) Database (https://www.ngdc.noaa.gov/mgg/shorelines/shorelines.html)
	Basin boundary data	N/A (vector data)	2020	Fujian Provincial Department of Water Resources
Socioeconomic survey data	Disaster bearer data (population, GDP, building area, crop area)	30 arc-seconds	2020	Fujian Provincial Emergency Department and Fujian Disaster Reduction Centre
	Disaster reduction capacity indicator data	County	2020	Fujian Provincial Emergency Department and Fujian Disaster Reduction Centre
Macroscale geospatial products	Digital elevation model (DEM)	30 m	2020	Data Center for Resources and Environmental Sciences (https://www.resdc.cn/)
	Land use and land cover (LULC)	30 m	2020	Data Center for Resources and Environmental Sciences (https://www.resdc.cn/)
	Road network data	N/A (vector data)	2020	OpenStreetMap Data https://www.openstreetmap.org
	River network data	N/A (vector data)	2020	OpenStreetMap Data https://www.openstreetmap.org
	Difference Vegetation Index	30 m	2020	Data Center for Resources and Environmental Sciences (https://www.resdc.cn/)
	Fracture zone data	N/A (vector data)	2020	Data Center for Resources and Environmental Sciences (https://www.resdc.cn/)
	Typhoon precipitation data	10 km	2009–2020	National data center for the Qinghai-Tibet plateau https://data.tpdc.ac.cn/en/data/8028b944-daaa-4511–8769–965612652c49
	Maximum inundation depth during storm surges	30 arc-seconds	2009–2020	Fujian Provincial Emergency Department and Fujian Disaster Reduction Centre

a subtropical monsoon climate zone and is located in the transition region between the Eurasian continent and the Northwestern Pacific, making it highly prone to typhoon impacts. As a result, typhoon disaster chains are diverse and occur frequently. The major types include Typhoon-Rainfall-Urban Waterlogging (TRU), Typhoon-Rainfall-Flood (TRF), Typhoon-Rainfall-Landslide (TRL), and Typhoon-Wind-Storm Surge (TWS), which jointly make Fujian one of the most typhoon-affected regions in China (Han et al., 2023; Yang et al., 2025). As of 2020, the province had a permanent population of 41.83 million. Administratively, it comprises nine prefecture-level cities and 84 county-level divisions, including the Pingtan Comprehensive Experimental Zone. A 30-arc-second (~1 km) grid system is employed in this study, covering 159,532 grid cells, to capture the fine-scale spatial heterogeneity of typhoon disaster-chain risks and their socio-natural driving mechanisms.

2.2. Data sources

This study integrates three categories of spatially explicit datasets to support the modeling of typhoon disaster-chain risks. The first

Table 2
Typhoon disaster chain risk assessment index system.

Factor	Abbreviation	Indicator	TRU	TRF	TRL	TWS	Reference
Hazard of disaster-inducing factors	ACP	Average cumulative precipitation (mm)	+	+	+	/	Mantovani et al., (2024); Lai et al., (2020); Wang and Nan, et al., (2024); Li et al., (2023)
	MCP	Maximum cumulative precipitation (mm)	+	+	+	/	
	ADP	Average number of days with daily precipitation $\geq$ 50 mm (d)	+	+	+	/	
	TDP	Total number of days with daily precipitation $\geq$ 50 mm (d)	+	+	+	/	
	MIS	Maximum inundation depth during storm surges (m)	/	/	/	+	
Sensitivity of disaster-forming environment	ELE	Elevation (m)	-	-	+	-	Dawit et al., (2023); Ye et al., (2022); Lin et al., (2012)
	Slope	Slope (°)	-	-	+	-	
	NDVI	Normalized Difference Vegetation Index	/	/	-	/	
	PC	Profile curvature	+	+	/	/	
	TWI	Topographic wetness index	+	+	/	/	
	ISR	Impervious surface ratio (%)	+	/	/	/	
	GSR	Green space ratio (%)	-	-	/	/	
	Relief	Relief (m)	-	/	+	/	
	DFZ	Distance to fault zones (m)	/	/	-	/	
	DCZ	Distance to coastal zones (m)	/	/	/	-	
	DR	Distance to rivers (m)	/	-	/	/	
	LUT	Land use type	/	/	/	+	
	SPI	Stream power index	/	+	/	/	
Exposure of disaster-bearing bodies	PD	Population density (people/km^2)	+	+	/	+	McMichael et al., (2020); Yang and Yusoff, et al., (2024); Cai et al., (2020); Li et al., (2023)
	GDP	GDP density (10 thousand yuan/km^2)	+	+	/	+	
	BUA	Built-up area (m^2/km^2)	+	+	/	+	
	CCA	Crop cultivation area (ha/km^2)	/	+	/	+	
Mitigation capacity for typhoon disasters	GDPS	Number of geological disaster prevention sites	/	/	-	/	Zhang and Chen, (2019); Cutter et al., (2008); Tu et al., (2022); Zhu et al., (2023); Hoque et al., (2018); Liu et al., (2022); Li et al., (2022); Qiao et al., (2024)
	GDMS	Number of geological disaster monitoring stations	/	/	-	/	
	MDMS	Number of marine disaster monitoring stations	/	/	/	-	
	MSD	Meteorological station density	-	-	-	-	
	HSD	Hydrological station density	-	-	/	/	
	ERC	Effective reservoir capacity (m^3)	/	-	/	/	
	PRDE	Number of people receiving disaster education	-	-	/	-	
	NHB	Number of hospital beds	-	-	-	-	
	SC	Shelter capacity (number of people)	-	-	-	-	
	ERS	Number of emergency rescue supplies	-	-	-	-	
	NE	Number of experts	-	-	-	-	

Note: "+ " indicates positive indicators, "-" indicates negative indicators, and "/" denotes unused indicators.

category includes basic geographic data, such as administrative boundaries and coastline information. The second category comprises socio-economic data, including population, GDP, cropland area, infrastructure, and census-derived statistics. The third category consists of geospatial products, including land-use datasets, digital elevation models, transportation networks, typhoon tracks, and precipitation records. To ensure spatial consistency, all datasets were resampled to a 30-arc-second (~1 km) resolution using bilinear interpolation. A detailed summary of the datasets is provided in Table 1.

2.3. Study framework

This study develops an analytical framework for assessing typhoon disaster-chain risks in Fujian Province using a unified 30-arc-second grid resolution. The framework consists of three major components: risk quantification, joint identification, and threshold-based mechanism analysis (Fig. 2). First, for the four representative disaster chain types—Typhoon-Rainfall-Urban Waterlogging (TRU), Typhoon-Rainfall-Flood (TRF), Typhoon-Rainfall-Landslide (TRL), and Typhoon-Wind-Storm Surge (TWS)—we construct a four-dimensional indicator system covering hazard, sensitivity, exposure, and mitigation capacity. Using a comprehensive weighting method, an integrated risk index is computed for each disaster chain. Second, joint exceedance probabilities are estimated using a Vine Copula model. A primary threshold of $\alpha = 0.90$ is applied, with $\alpha = 0.85$ and 0.95 used for sensitivity testing. Based on these probabilities, the spatial patterns and types of single disaster chains (SDCs) and compound disaster chains (CDCs) are identified. Population, GDP, and vulnerable population data are then used to evaluate the area distribution and exposure inequality of high-risk regions. Third, XGBoost models are trained for each disaster chain type, and SHAP values are used to quantify the importance of driving factors. Thresholds of dominant factors are extracted from SHAP dependence curves to capture nonlinear risk responses. Finally, for transition pathways with sufficient sample sizes (grid count > 10), a transition model is developed to examine the shift from single chains to compound chains. Using the combined XGBoost–SHAP approach, key drivers and their critical thresholds are identified, thereby clarifying the conditions under which compound disaster chains emerge.

2.4. Evaluation indicator system

This study establishes an evaluation indicator system for typhoon disaster chains consisting of four dimensions and 33 secondary indicators: the hazard of disaster-inducing factors (5 indicators), the sensitivity of the disaster-forming environment (13 indicators), the exposure of disaster-bearing bodies (4 indicators), and the mitigation capacity for typhoon disasters (11 indicators). It is worth noting that the typhoon rainfall hazard indicator is derived from 29 typhoons that caused documented losses in Fujian between 2009 and 2020 (Yang et al., 2025). For each event, precipitation within a 500-km radius of the typhoon center was defined as typhoon-related rainfall, and the hazard was quantified based on cumulative rainfall amounts and the number of days with 24-hour precipitation $\geq$ 50 mm (Jiang and Zipser, 2010). A detailed description of all indicators is provided in Table 1.

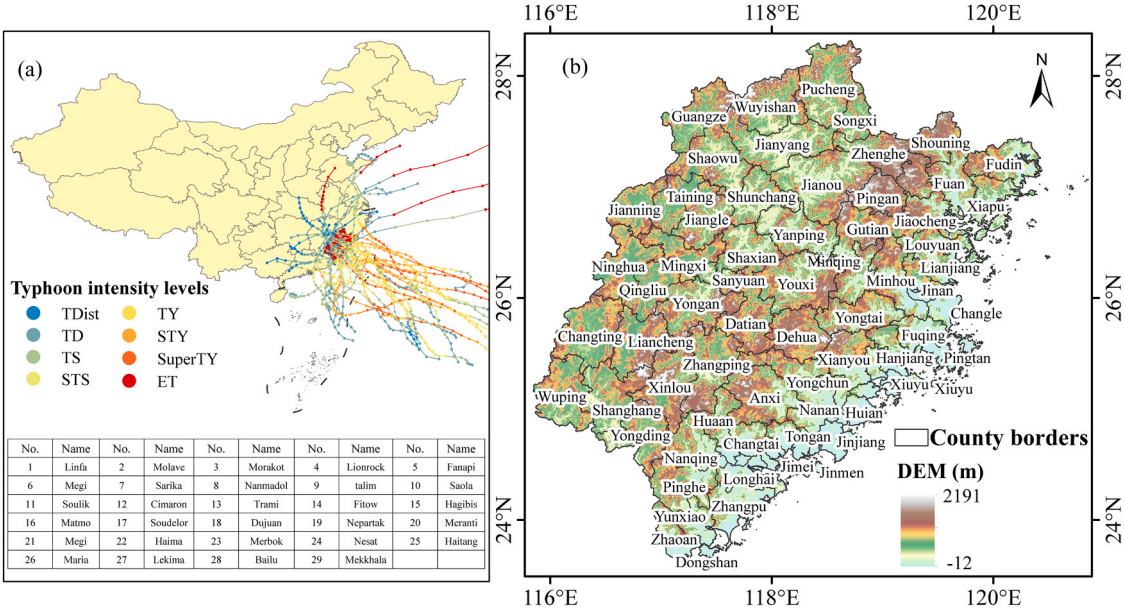

No.	Name	No.	Name	No.	Name	No.	Name	No.	Name
1	Linfa	2	Molave	3	Morakot	4	Lionrock	5	Fanapi
6	Megi	7	Sarika	8	Nanmadol	9	talim	10	Saola
11	Soulik	12	Cimaron	13	Trami	14	Fitow	15	Hagibis
16	Matmo	17	Soudelor	18	Dujuan	19	Nepartak	20	Meranti
21	Megi	22	Haima	23	Merbok	24	Nesat	25	Haitang
26	Maria	27	Lekima	28	Bailu	29	Mekkhala		

Fig. 1. Location of the study area. (a) Tracks and intensity levels of 29 typhoons that caused losses in Fujian between 2009 and 2020. (b) Digital Elevation Model (DEM) and county-level administrative boundaries of Fujian Province.

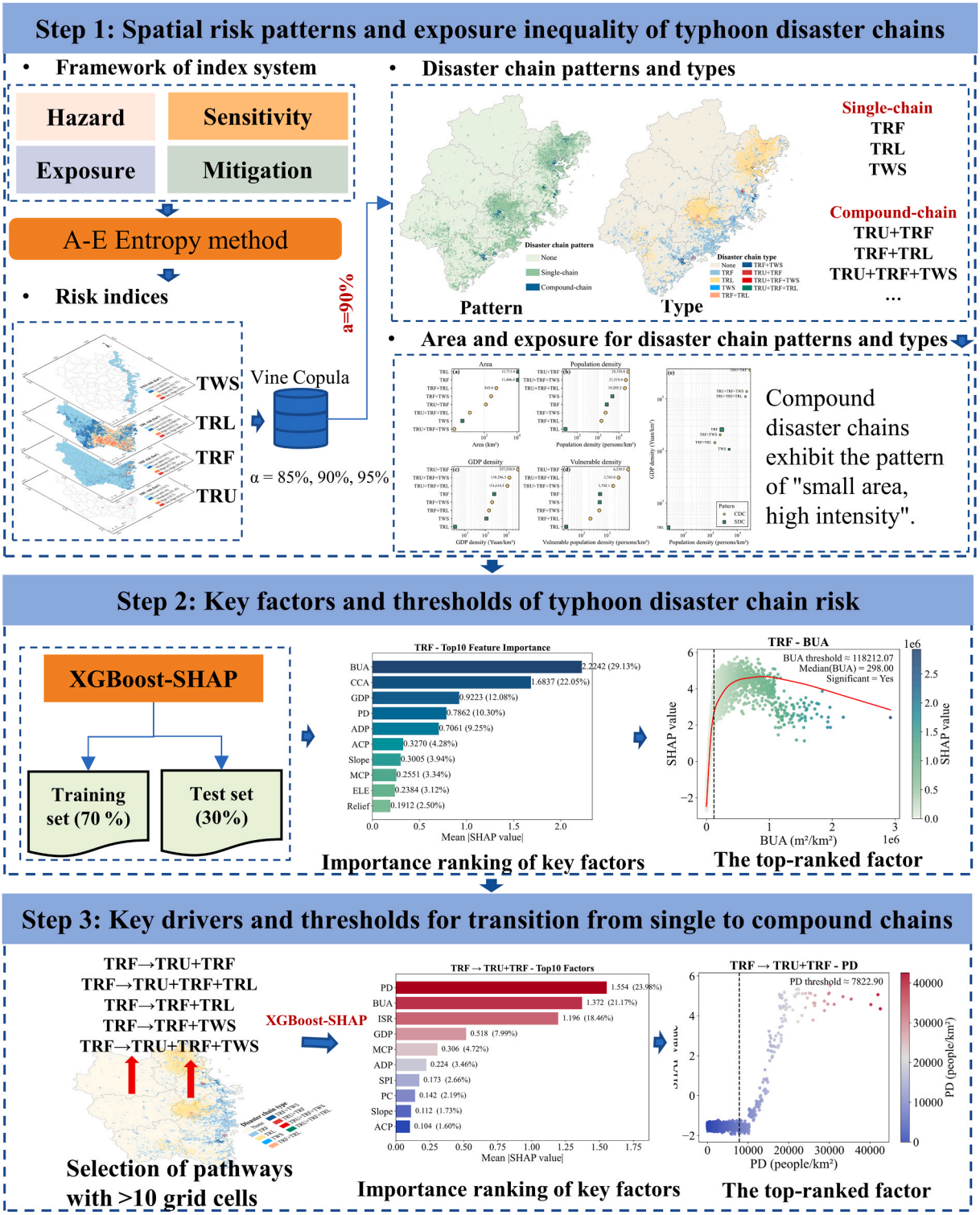

Fig. 2. Technical workflow of the study.

2.5. *Typhoon disaster chain risk and exposure assessment*

To systematically evaluate typhoon disaster chain risks, this study applies an integrated weighted assessment framework at the grid-cell scale. The framework incorporates four core dimensions: hazard of disaster-inducing factors (H), sensitivity of the disaster-

forming environment (S), exposure of disaster-bearing bodies (E), and mitigation capacity for typhoon disasters (M), as defined by the indicator system in Table 1.

All raw indicator data were first normalized using the min–max scaling method to eliminate dimensional inconsistencies and ensure comparability across indicators. For positive indicators, where larger values indicate higher risk, normalization was performed as:

$$x'_{ij} = \frac{x_{ij} - \min(x_j)}{\max(x_j) - \min(x_j)} \tag{1}$$

For negative indicators, where larger values imply lower risk, normalization was expressed as:

$$x'_{ij} = \frac{\max(x_j) - x_{ij}}{\max(x_j) - \min(x_j)} \tag{2}$$

where x_{ij} denotes the original value of indicator j in grid cell i, and x'_{ij} is the normalized value.

To balance expert knowledge and data-driven objectivity, indicator weights were determined using a combined Analytic Hierarchy Process (AHP) and entropy weight method. The AHP was used to derive subjective weights by structuring indicators hierarchically and constructing pairwise comparison matrices based on expert judgment. The relative importance of indicators was assessed using a nine-point scale (Yang et al., 2025). The normalized eigenvector corresponding to the maximum eigenvalue of each comparison matrix was taken as the subjective weight vector w_j^{AHP}. Consistency of judgments was evaluated using the consistency ratio (CR), and only matrices with $CR < 0.1$ were accepted.

The entropy weight method was employed to derive objective weights by quantifying the amount of information contained in each indicator based on its spatial variability. The entropy value of indicator j was calculated as:

$$e_j = -k \sum_{i=1}^{n} p_{ij} \ln(p_{ij}) \tag{3}$$

where $p_{ij} = \frac{x'_{ij}}{\sum_{i=1}^{n} x'_{ij}}$, n is the number of grid cells, and $k = 1/\ln(n)$. The degree of divergence was then computed as $d_j = 1 - e_j$, and the objective weight was obtained as:

$$w_j^{ENT} = \frac{d_j}{\sum_{j=1}^{m} d_j} \tag{4}$$

where m is the number of indicators.

To integrate subjective and objective information in indicator weighting, this study combines the weights derived from the Analytic Hierarchy Process (AHP) and the entropy weight method using a similarity-based approach following (Yang et al., 2025). The basic idea is to determine combination coefficients by characterizing the discrepancy between the two weight vectors and then constructing composite weights through weighted averaging.

Let w'_i and w''_i denote the subjective weight obtained from AHP and the objective weight obtained from the entropy method for indicator i, respectively. The discrepancy between the two weight sets is quantified using a squared distance measure, expressed as:

$$\frac{1}{2} \sum_{i=1}^{n} (w'_i - w''_i)^2 = (\alpha - \beta)^2 \tag{5}$$

where n is the number of indicators, and α and β are the combination coefficients reflecting the relative contributions of the two weighting schemes.

The combination coefficients are subject to the following constraint:

$$\alpha + \beta = 1,\ \alpha > 0, \beta > 0 \tag{6}$$

Based on the estimated coefficients, the composite weight for indicator i is calculated as a linear combination of the two original weights:

$$w_i = \alpha w'_i + \beta w''_i \tag{7}$$

where w_i represents the final composite weight used in the subsequent risk assessment. This weighting strategy allows both expert judgment and data-driven information to be incorporated into the indicator system, thereby improving the robustness and interpretability of the composite index.

For the risk index calculation, weighted aggregation was performed at the grid-cell scale to obtain the indices of H, S, E, and M. Considering the nonlinear suppressing effect of M on overall disaster risk, an exponential function was introduced to construct the comprehensive typhoon disaster chain risk index (R), expressed as:

$$R = H \times S \times E \times (1 - M) \tag{8}$$

This formulation integrates hazard intensity, environmental sensitivity, exposure level, and the attenuating effect of mitigation capacity.

To quantify the concentration of socioeconomic exposure within high-risk areas, this study calculates the exposure lift value (Lift) for both population and GDP. Lift is defined as the ratio of exposure density within the high-risk area of a given disaster chain to the provincial average exposure density (Peduzzi et al., 2009):

$$Lift = D_h / D_O \tag{9}$$

where$D_h$is the population (or GDP) density within the high-risk area of a given disaster chain, and$D_o$is the provincial average density. This ratio removes the influence of area size; a higher lift value indicates a stronger concentration of socioeconomic exposure per unit area, reflecting a more pronounced risk amplification effect.

2.6. Joint probability of disaster chains

Building on the risk index results, we quantify the coexistence characteristics and statistical dependencies among multiple disaster chains using a Copula-based joint probability modeling approach (Frahm et al., 2005; Aas et al., 2009; Ganguli and Merz, 2024).

First, the empirical cumulative distribution function (ECDF) was used to transform the observed intensity of each disaster chain into marginal probabilities following a uniform distribution:

$$\widehat{U}_k = F_k(x) = \frac{1}{n}\sum_{i=1}^{n}\prod(X_i \le x) \tag{10}$$

where$\widehat{U}_i$denotes the marginal probability of disaster chain$k$,$F_k$is its empirical distribution function, and$\prod$is the indicator function.

Multiple thresholds (α= 0.85, 0.90, 0.95) were then applied to determine which disaster chains exceed the threshold within each grid cell. Based on these exceedances, grid cells were classified into single-chain, compound-chain, or non-risk categories, revealing the spatial patterns of extreme events.

To characterize the nonlinear and tail dependence among disaster chains, a Vine Copula model was employed. Vine Copulas hierarchically organize pairwise Copula components and effectively capture multivariate, asymmetric, and nonlinear dependence structures. Among several candidate Copula families (Clayton, Gumbel, Frank, Student-t, and Gaussian), the optimal structure was selected using the Akaike Information Criterion (AIC):

$$AIC = -2.\log(L) + 2k \tag{11}$$

where$L$is the likelihood and$k$is the number of parameters.

Using the fitted Vine Copula structure, large-scale Monte Carlo sampling was performed to estimate the joint exceedance probability for a given threshold$a$:

$$P(\cap\{U_k > a\}) \tag{12}$$

Conditional probabilities were also computed to evaluate the likelihood of one disaster occurring given that another has already occurred:

$$P(U_i > a | U_j > a) = \frac{P(U_i > a, U_j > a)}{P(U_j > a)} \tag{13}$$

Based on the joint probability results, a classification procedure was established to identify high-risk areas. For a given threshold (e.g.,$a = 0.90$), each grid cell is classified as follows: if all disaster-chain probabilities fall below the threshold, the cell is defined as a non-significant risk zone; if exactly one disaster-chain probability exceeds the threshold, it is classified as a single-chain zone; and if two or more exceed the threshold simultaneously, it is categorized as a compound-chain zone. This classification provides the foundation for subsequent analyses of spatial patterns and exposure inequality.

2.7. Explainable analysis of disaster chain formation mechanisms

To identify the key driving factors and their functional roles in shaping the spatial patterns of different typhoon disaster chains, we applied model interpretability methods based on machine learning. Classification models were developed for the eight major disaster-chain categories (including both single disaster chains and compound disaster chains) to evaluate the importance of each feature (Dey and Haque, et al., 2024; Wang and Nan, et al., 2024; Li et al., 2022).

First, using the disaster-chain maps derived from the α = 0.90 threshold, environmental and hazard-related variables were extracted for all grid cells belonging to each disaster chain category, forming the feature dataset. For each category, a binary classifier was trained to determine the probability that a given grid cell belongs to that disaster-chain type.

XGBoost was used to build the classification models. The prediction function is:

$$\widehat{y}_i = \phi\left(\sum_{k=1}^{k} f_k(X_i)\right) \tag{14}$$

where f_k is the k-th decision tree, ϕ is the sigmoid function, and X_i is the feature vector. Key hyperparameters were set as follows: n_estimators = 250, learning_rate = 0.05, max_depth = 4, subsample = 0.8, colsample_bytree = 0.8. The dataset was randomly split into training and testing subsets at a 70:30 ratio using stratified sampling to maintain class balance.

To quantify each feature's contribution to the model predictions, SHAP (SHapley Additive exPlanations) values were computed. Based on cooperative game theory, SHAP assigns each feature a marginal contribution for each sample. The SHAP value for feature i is defined as:

$$\phi(X) = \sum_{S \subseteq N \setminus \{j\}} \frac{|S|!(M - |S| - 1)!}{M!} [f(S \cup \{j\}) - f(S)] \tag{15}$$

where N is the set of all features, M is the total number of features, and S is any subset of features that does not include feature i.

Features were ranked according to the mean absolute SHAP value to identify the dominant factors.

$$\frac{1}{n}\sum_{i=1}^{n} |\phi_j(X_i)| \tag{16}$$

For the dominant factors, nonlinear effects and interactions with model decisions were further examined using locally weighted scatterplot smoothing (LOWESS). The response curve is expressed as:

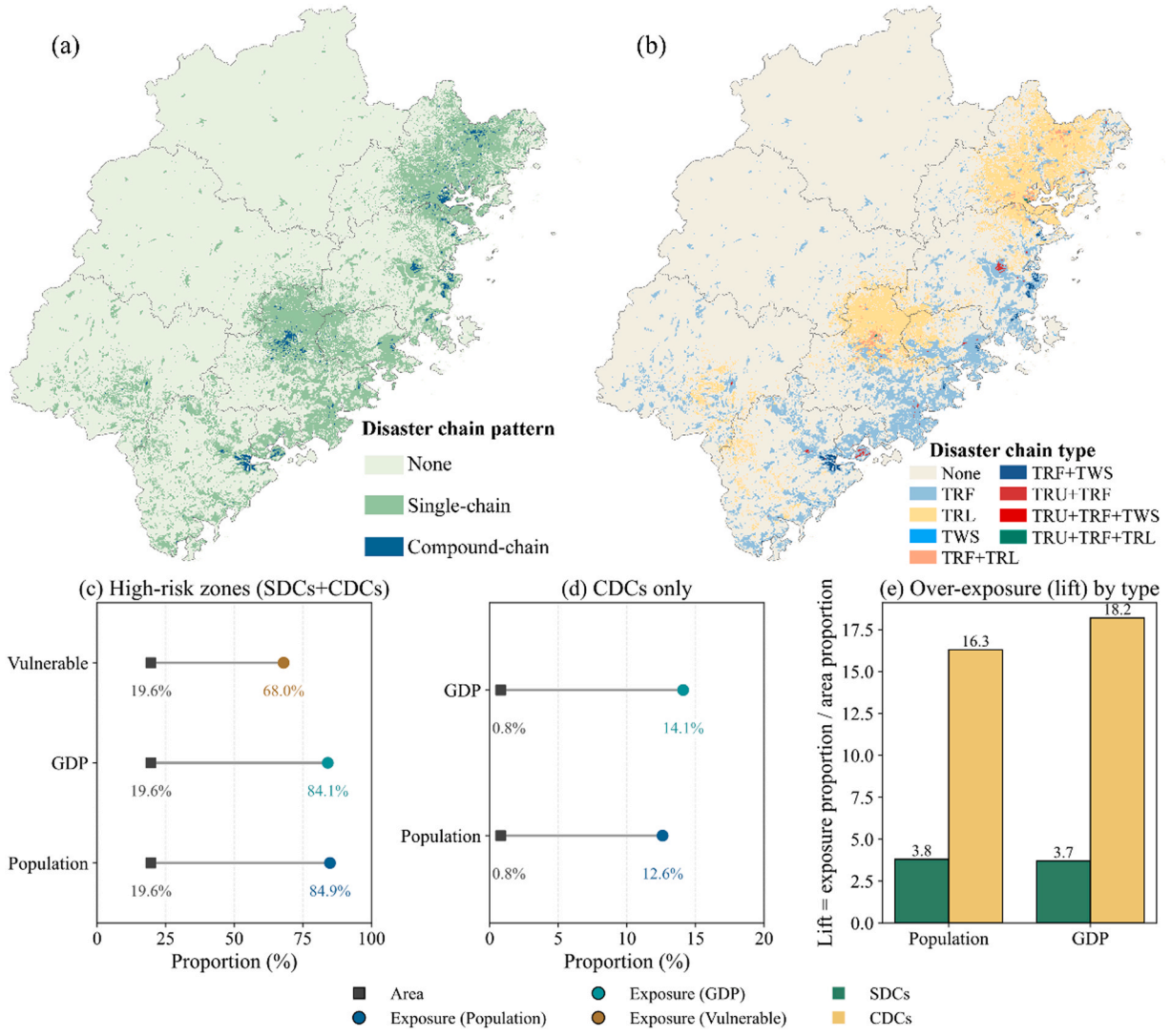

Fig. 3. Typhoon disaster chain patterns, combination types, and exposure metrics (90 % exceedance threshold). (a) Spatial distribution of disaster chain patterns; (b) Distribution of disaster chain types; (c) Proportions of area, population, GDP, and vulnerable population within high-risk zones (SDCs + CDCs); (d) Population and GDP exposure proportions within CDCs; (e) Comparison of exposure lift values between SDCs and CDCs.

$$y_i = g(x_i) + \varepsilon_i \tag{17}$$

where$g(.)$is the local regression function, and$\varepsilon_i$is the random error. Gradients within the 5 %–95 % quantile range were computed:

$$x^* = \underset{x}{\operatorname{argmax}} \left| \frac{dg(x)}{dx} \right| \tag{18}$$

to detect threshold pointsx^*. A *t*-test was applied to examine whether SHAP values significantly differed from zero$(H_0 : \mu_\phi = 0)$:

$$\mathrm{t} = \frac{\overline{\phi}}{s/\sqrt{n}} \tag{19}$$

where$\overline{\phi}$is the sample mean of SHAP values,$s$is the standard deviation, and$n$is the sample size.

To investigate the mechanisms governing transitions from single disaster chains to compound disaster chains, representative compound chain types with more than 30 grid cells (e.g., TRF → TRF+TRL, TRF → TRF+TWS) were selected. For each transition pathway, a dedicated binary classifier was constructed, and piecewise linear fitting (PWLF) was applied to identify critical thresholds for key driving variables. These thresholds represent turning points that signal the onset of compound-chain formation.

It is important to note that SHAP provides post-hoc explanations based on game theory and reflects stable associations within the trained model; it does not establish strict causal relationships. Accordingly, the threshold and turning-point values identified in this study, which are derived from SHAP dependence patterns, LOWESS smoothing, and piecewise linear fitting, should be interpreted as approximate statistical turning points rather than exact physical critical values. The purpose of this analysis is to provide data-driven insights into the mechanisms underlying typhoon disaster chain formation and to support the development of mechanistic hypotheses, rather than to define deterministic thresholds.

3. Results

3.1. Spatial patterns of typhoon disaster chain risks and exposure inequality

To examine the spatial patterns of typhoon disaster chain risks across Fujian Province, a Copula-based joint probability model was applied using the 90 % exceedance probability as the threshold for identifying high-risk areas. Under this criterion, each grid cell was classified into one of three categories: no significant risk, single disaster chains (SDCs), and compound disaster chains (CDCs) (Fig. 3a). Eight typical disaster chain combinations were identified within high-risk zones, each exhibiting distinct joint probability

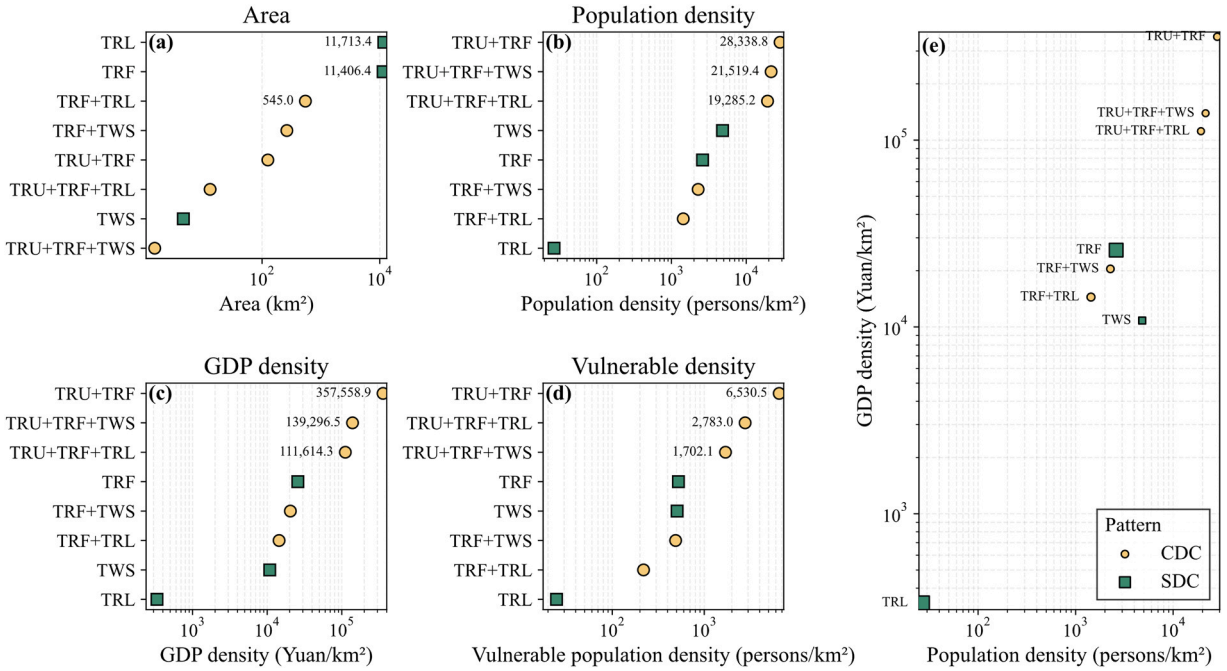

Fig. 4. Comparison of area and exposure density metrics across different disaster chain types (single and compound disaster chains). (a–d) Cleveland dot plots ($\log_{10}$ scale on the x-axis) showing the area, population density, GDP density, and vulnerable population density for each disaster chain type. (e) Log–log bubble chart comparing population density and GDP density; bubble size represents spatial extent, and colors distinguish single disaster chains (SDCs) from compound disaster chains (CDCs).

characteristics (Fig. 3b). The mean joint occurrence probability of CDCs (0.0082) is 13.6 times higher than that of SDCs (0.0006), and the maximum joint probability of CDCs (0.7449) also exceeds that observed for SDCs (0.5032). In addition, the mean probability that at least one hazard occurs within CDCs reaches 0.9977, slightly higher than the corresponding value for SDCs (0.9755), indicating that multi-hazard interactions are associated with elevated hazard occurrence likelihoods. Among all identified combinations, the compound chain comprising Typhoon–Rainfall–Urban Waterlogging (TRU), Typhoon–Rainfall–Flood (TRF), and Typhoon–Wind–Storm Surge (TWS) exhibits a relatively high mean joint probability (0.6133), exceeding expectations under an independence assumption and suggesting positive dependence among these processes. Although the overall mean joint probability of the TRU + TRF combination is relatively low (0.006), its local maximum reaches 0.5738, indicating pronounced spatial heterogeneity and localized areas of elevated compound risk.

Spatially, SDCs are mainly distributed in transitional zones from coastal to inland regions, forming a continuous background risk belt along major coastlines, river valleys, and the foothills of low mountains (Fig. 3a–b). In contrast, CDCs exhibit distinct clustering patterns, with concentrations in coastal metropolitan centers such as Fuzhou, Xiamen, and Quanzhou, as well as in bay–river–city transition zones. Although high-risk areas (SDCs + CDCs) account for only 19.6 % of the provincial land area, they contain 84.9 % of the population, 84.1 % of the GDP, and 68.0 % of the vulnerable population (Fig. 3c), reflecting a concentration of exposure within a limited spatial extent. CDCs alone occupy only 0.8 % of all high-risk areas but include 12.6 % of the population and 14.1 % of the GDP (Fig. 3d). Their exposure lift values for population and GDP reach 16.3 and 18.2, respectively, substantially higher than the corresponding values for SDCs (3.8 and 3.7; Fig. 3e). These results indicate that compound disaster chains, while spatially limited, are closely associated with disproportionately high concentrations of population and economic assets in highly urbanized coastal settings.

Significant disparities in risk exposure are observed across different disaster-chain patterns. Within CDCs, the TRU + TRF combination occupies only 125.4 km^2 (13.2 % of all CDC areas), yet it exhibits the highest population, GDP, and vulnerable population densities in the province, reaching 11.4, 29.1, and 18.6 times the corresponding averages of SDCs, respectively (Fig. 4a–d). In the log–log bubble plot, TRU + TRF is located in the upper-right quadrant while maintaining the smallest spatial footprint, indicating a distinct configuration characterized by high exposure intensity within a limited area (Fig. 4e). In contrast, compound disaster chains without TRU involvement, such as TRF + TRL and TRF + TWS, generally exhibit moderate exposure densities. Furthermore, although high-risk zones associated with TRL contain relatively small total populations, the proportion of vulnerable population within these areas reaches 92.1 %. This pattern indicates that, outside CDC-dominated zones, the composition of exposed populations plays an important role in shaping overall social risk levels. Overall, these results highlight pronounced heterogeneity in exposure intensity and

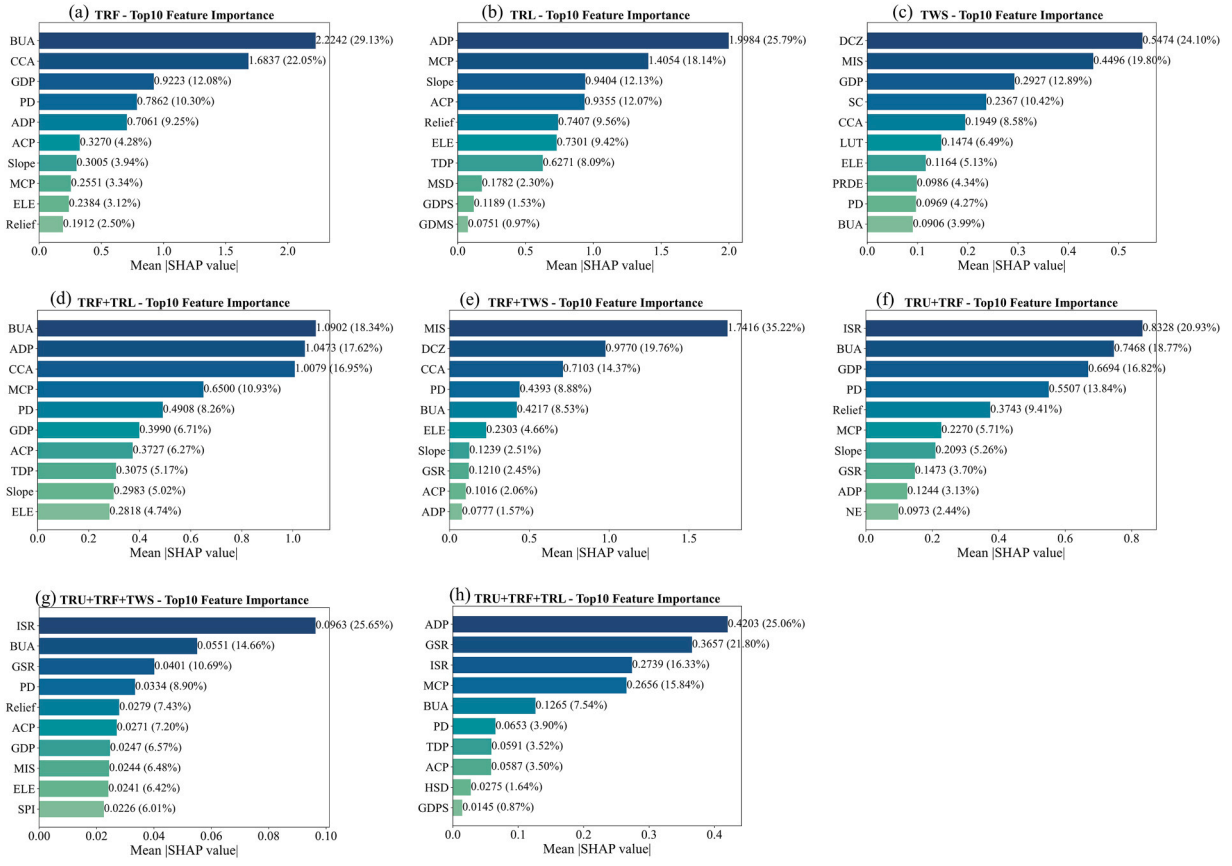

Fig. 5. Relative SHAP importance (%) of the top 10 factors across high-risk areas for different typhoon disaster chain types.

vulnerability composition across different disaster chain types.

3.2. Key driving factors and threshold characteristics of typhoon disaster chain risks

Results from the XGBoost–SHAP analysis indicate that high-risk areas of typhoon disaster chains are shaped by the combined effects of natural triggering conditions and subsequent social amplification processes. Natural factors primarily define the baseline environmental conditions under which hazards are initiated, whereas land-use intensity and the concentration of population and economic activities largely determine the magnitude of risk amplification. Across all disaster chain types, the cumulative contribution of social factors exceeds that of natural factors (Fig. 5), highlighting the dominant role of human-modified environments in controlling the spatial distribution of disaster chain risks.

For the TRF chain, built-up area (BUA, 29.13 %), crop cultivation area (CCA, 22.05 %), and population density (PD, 10.30 %) together contribute more than the average number of days with daily precipitation ≥ 50 mm (ADP, 9.25 %) (Fig. 5a). This pattern indicates that spatial variations in flood risk are more strongly associated with land-use intensity and socioeconomic exposure than with rainfall persistence alone. In contrast, the TWS chain is more strongly controlled by natural factors. Distance to coastal zones (DCZ, 24.10 %) and maximum inundation depth during storm surges (MIS, 19.80 %) are the most influential drivers (Fig. 5c), reflecting the importance of nearshore exposure and coastal hydrodynamic forcing. Nevertheless, GDP density (GDP) and population density (PD) also contribute appreciably, indicating that coastal risk levels are jointly shaped by hydrodynamic processes and human exposure. For compound disaster chains such as TRF + TWS, MIS remains the dominant factor (35.22 %), while the combined contributions of CCA, BUA, and PD exceed 31 % (Fig. 5e), highlighting the amplifying role of land-use intensity and population exposure in compound coastal flooding. In compound chains involving TRU, the dominance of social controls becomes even more pronounced. For example, in the TRU + TRF chain, impervious surface ratio (ISR, 20.93 %), together with BUA, GDP, and PD, accounts for nearly half of the total importance (Fig. 5f–g), underscoring the critical role of urban surface sealing and built-environment intensity in

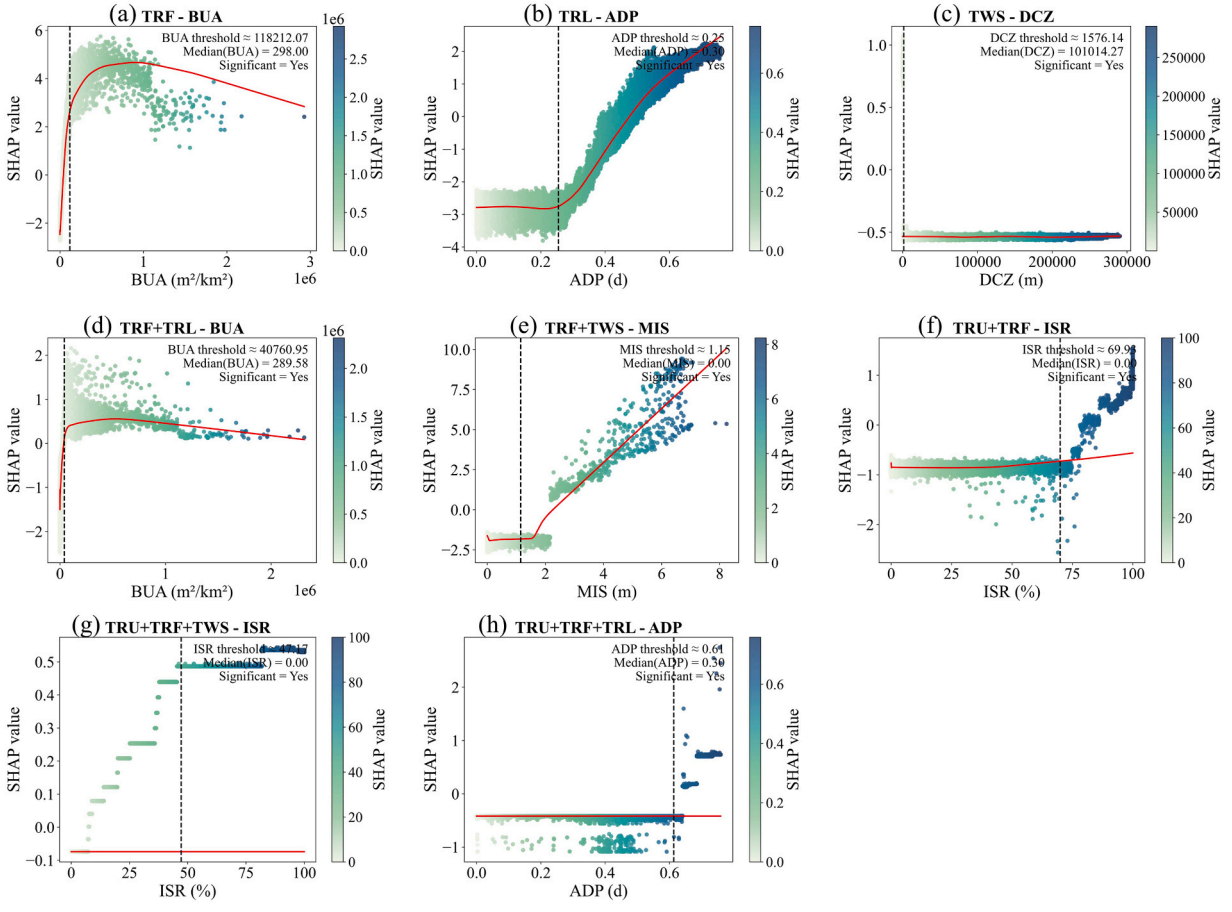

Fig. 6. SHAP dependence plots and threshold characteristics for each typhoon disaster chain type in high-risk areas. Dots represent the SHAP values of individual samples, with colors indicating the original values of the corresponding feature (or the strongest interacting feature). The red line shows the LOWESS-smoothed trend, and the gray dashed line marks the threshold, identified through PDP/ICE analysis or the turning point of the SHAP response curve.

intensifying multi-hazard interactions.

Different disaster chain types further exhibit clear nonlinear threshold behaviors in their dominant driving factors. Threshold analysis shows that risk contributions increase sharply once key variables exceed specific critical values (Fig. 6). In the TRF chain, flood risk increases markedly when BUA exceeds approximately 118,212.07 m^2/km^2 (Fig. 6a), indicating a transition from rainfall-dominated flooding to urban-amplified flooding. In the TRL chain, ADP exhibits a threshold of about 0.25 days (Fig. 6b), beyond which landslide-related risk increases rapidly. For the TWS chain, the response threshold for DCZ is approximately 1576.14 m (Fig. 6c), highlighting the importance of nearshore proximity for storm-surge impacts. In the compound TRF + TWS chain, MIS shows a threshold near 1.15 m (Fig. 6e), reflecting the critical role of surge intensity in compound coastal flooding. For compound chains involving TRU, ISR exhibits a threshold range of 47 %–70 % (Fig. 6f–g), suggesting that surface sealing substantially enhances hazard interactions once urbanization exceeds this level. Notably, when ADP exceeds 0.61 days, the occurrence probability of the TRU + TRF + TRL compound chain increases sharply (Fig. 6h), indicating that persistent heavy rainfall acts as a key trigger for the emergence of highly complex disaster chain configurations.

3.3. *Transition mechanisms and critical thresholds from single to compound disaster chains*

To clarify how single disaster chains evolve into compound configurations, five representative transition pathways with sufficient spatial samples (grid count > 10) were analyzed. Based on the XGBoost–SHAP importance results (Fig. 7), these transition mechanisms can be grouped into two dominant modes: socioeconomically driven pathways and naturally driven pathways. Socioeconomically driven transitions are mainly associated with TRU-related compound chains, whereas naturally driven transitions are primarily linked to TRL- and TWS-related compound chains. This distinction reflects systematic differences in how human-modified environments and natural processes govern the formation of compound disaster chains.

For TRU-related transitions, population density (PD) plays a leading role. In the TRF → TRU + TRF pathway, PD accounts for 23.98 % of the total importance, with built-up area (BUA) and impervious surface ratio (ISR) acting as secondary contributors (Fig. 7a). This pattern indicates that population concentration and urban surface characteristics facilitate the coupling of fluvial flooding and urban waterlogging. In the more complex TRF → TRU + TRF + TRL transition, the dominant control shifts to BUA (28.33 %) (Fig. 7b), reflecting the increasing influence of built-environment intensity in enabling cascading interactions between urban flooding and slope-related hazards. In contrast, transitions involving TRL and TWS are primarily governed by natural drivers. The TRF → TRF + TRL pathway is mainly controlled by ADP (12.83 %) (Fig. 7c), whereas the TRF → TRF + TWS transition is dominated by MIS (40.97 %) (Fig. 7d). For the more complex TRF → TRU + TRF + TWS pathway, both stream power index (SPI, 14.23 %) and MIS (11.76 %) exert strong influences (Fig. 7e), indicating joint controls from fluvial erosive processes and coastal hydrodynamics. Across TRL- and TWS-related pathways, elevation (ELE) consistently acts as a background control factor by constraining runoff convergence, slope stability, and indirectly modulating exposure to coastal inundation.

Threshold analysis further quantifies the critical conditions under which these transitions occur (Fig. 8). For socioeconomically driven transitions, the TRF → TRU + TRF pathway exhibits a population density threshold of approximately 7822.90 persons/km^2 (Fig. 8a). The TRF → TRU + TRF + TRL transition is governed by built-up area, with a threshold of 587,617.01 m^2/km^2 (Fig. 8b), indicating a critical level of urban development beyond which slope-related hazards are more likely to be coupled with flooding. For naturally driven transitions, the thresholds for the TRF → TRF + TRL and TRF → TRF + TWS pathways are 0.46 days of ADP and

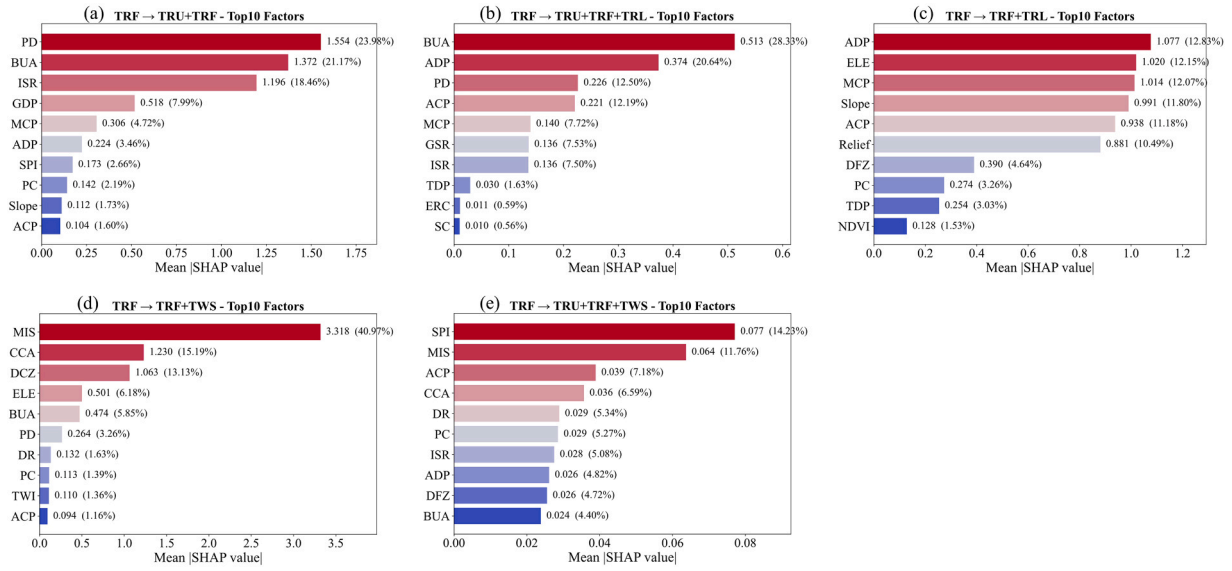

Fig. 7. Top 10 most important driving factors for transitions from single to compound disaster chains.

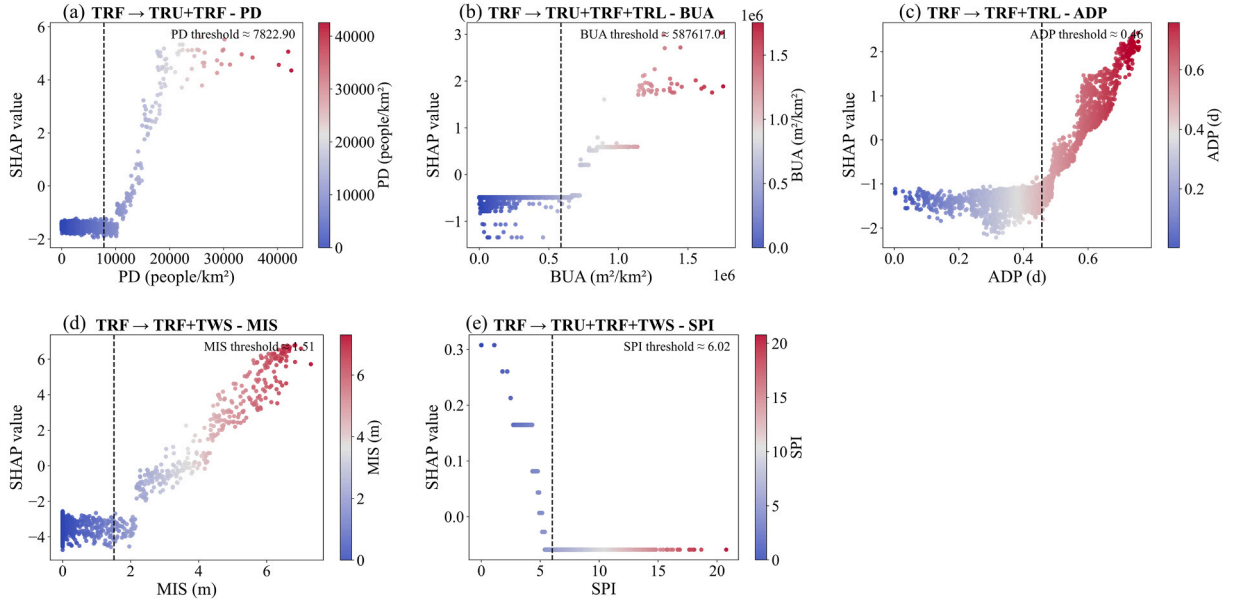

Fig. 8. Threshold characteristics of key driving factors in the transition from single to compound disaster chains.

1.51 m of MIS, respectively (Fig. 8c–d). In the more complex TRF → TRU + TRF + TWS transition, the key threshold corresponds to a stream power index value of 6.02 (Fig. 8e), representing a critical level of runoff concentration and erosive energy. Collectively, these results indicate that urbanization intensity (BUA and PD), rainfall persistence (ADP), and nearshore hydrodynamic conditions (MIS and SPI) constitute the fundamental controls governing transitions from single to compound disaster chains.

4. Discussion

4.1. Socio-natural coupling mechanisms driving typhoon disaster chain risks

By integrating joint probability analysis with explainable machine learning, this study demonstrates that typhoon disaster chain risks emerge through a socio–natural coupling process characterized by natural triggering and social amplification (Ganguli and Merz, 2024). This perspective extends traditional risk analysis frameworks that focus on single hazards or linear trigger–response relationships. The results indicate that nonlinear interactions between hazard intensity and socioeconomic exposure constitute a key mechanism driving the amplification of compound disaster chain risks. Accordingly, disaster risk assessment should not only consider whether hazards occur, but also systematically examine how hazard intensity, inter-hazard dependence, and compound behavior develop under specific socio-geographical conditions. This perspective is consistent with current directions in international disaster risk research (Ganguli and Merz, 2024; Deb et al., 2023).

However, existing studies largely concentrate on individual hazard processes, specific types of compound events (e.g., rainfall–-storm surge flooding), or rely on high-resolution physical models to simulate localized processes. These approaches face inherent limitations in capturing multi-hazard chain combinations, spatial exposure disparities, and the mechanisms governing transitions from single to compound disaster chains at regional scales (Meng et al., 2025; Ganguli and Lin., 2025). In contrast, this study integrates joint occurrence probabilities, socioeconomic exposure patterns, and disaster-chain transition mechanisms within a unified regional framework. This integrated approach reveals the overall logic through which typhoon disaster chain risks evolve from natural triggering to social amplification, thereby advancing disaster-chain research from event-based analysis toward system-level risk identification.

From a methodological perspective, this study complements previous approaches based on physical process modeling or single-hazard assessments. Two- and three-dimensional hydrodynamic models are effective for simulating floods and storm surges, but their strong dependence on high-quality data and computational resources limits their application to long time series, multiple scenarios, and multi-hazard combinations at regional scales (Lockwood et al., 2024; Liu et al., 2022). Purely data-driven methods offer high computational efficiency but often lack interpretability regarding hazard dependence and driving mechanisms. By combining Copula-based joint probability models with explainable machine learning, this study achieves a balance between statistical robustness and interpretability, enabling systematic identification of multi-hazard dependence structures, key driving factors, and critical thresholds.

The results show that the joint occurrence probability of compound disaster chains is significantly higher than expected under independence assumptions, confirming strong positive dependence among hazard processes (Moftakhari et al., 2017; Naseri and Hummel, 2022). Risk patterns also exhibit pronounced spatial heterogeneity and social disparity. Compound disaster chain risks are

strongly amplified in highly urbanized areas, while in single-chain typhoon–rainfall–landslide (TRL) high-risk zones, vulnerable populations account for up to 92.1 % of residents. This pattern indicates that disaster risk is shaped not only by physical hazard conditions but also by social vulnerability structures (Jiang et al., 2023; Morita et al., 2017). Under rapid urbanization, the impervious surface ratio emerges as a key control factor for typhoon–rainfall–urban waterlogging (TRU)–related compound chains. When impervious surface coverage exceeds approximately 65–70 % under high building density, risk levels increase nonlinearly. This suggests that urbanization can substantially enhance the joint occurrence of flooding and waterlogging by reducing infiltration capacity and constraining natural drainage pathways (Feng et al., 2023; Javed et al., 2025). Overall, natural factors define the background conditions for hazard triggering, whereas social factors dominate the amplification of disaster chain risks. These findings support a shift from hazard-centered approaches toward integrated socio–ecological system frameworks that emphasize coupling mechanisms and threshold identification (Naseri and Hummel, 2022; Peduzzi et al., 2012; Cramer et al., 2018).

4.2. Implications for managing typhoon disaster chains

The spatial patterns identified in this study reveal a clear contrast between the widespread distribution of single disaster chains and the strong clustering of compound disaster chains. This finding indicates that conventional disaster prevention strategies—often designed around single hazards or homogeneous regions—are insufficient for addressing the spatial concentration and mechanism diversity of compound disaster chain risks. Accordingly, typhoon disaster chain management should shift from hazard-type-centered approaches toward differentiated risk control frameworks based on disaster-chain combinations and exposure structures. Such frameworks emphasize zone-specific and chain-specific strategies that reflect regional differences in hazard composition, exposure density, and dominant driving mechanisms, thereby improving the efficiency and effectiveness of disaster risk reduction.

In highly urbanized coastal clusters such as Fuzhou, Xiamen, and Quanzhou, compound disaster chain risks are strongly concentrated, and exposure levels are unlikely to decrease in the short term. In these areas, the primary management objective is not to reduce exposure, but to enhance system-level resilience and coordinated defense capacity. Priority should be given to the functional integration of engineering systems, coordinated governance, and gradual optimization of urban spatial structure. Existing flood control and drainage systems can be progressively upgraded toward integrated configurations that combine flood protection, storm surge defense, and urban drainage, aligned with maintenance and renewal cycles (Mohtat and Khirfan, 2022; Zhang et al., 2025; Alfieri et al., 2020). At the same time, improving drainage standards, expanding distributed detention and retention facilities, and advancing sponge-city measures can enhance urban stormwater regulation in a cost-effective manner (Liang et al., 2024). Strengthening coordination between meteorological, hydrological, and urban management systems is also essential. Integrated disaster-chain response mechanisms and regular scenario-based exercises for high-risk combinations such as TRU and TRF can improve cross-sector emergency response capacity (Yu et al., 2023). In spatial planning, stricter controls on new development in low-lying areas and flood pathways, together with gradual spatial optimization during urban renewal, can reduce the amplification potential of compound disaster chains (Wang and Nan, et al., 2024; Yang and Qin., 2024).

In peripheral regions such as Ningde and parts of Quanzhou, where compound disaster chain risks are emerging, proactive planning and development constraints are critical. As urban expansion extends into hilly and mountainous areas, disaster control zones should be clearly defined at the planning stage. Development on high-risk slopes should be restricted, and ecological slope protection and drainage systems should be implemented simultaneously to enable integrated risk management from hillslopes to urban areas (Zhuang et al., 2023; Liang et al., 2022). In extensive areas dominated by single disaster chains, management strategies should focus on dominant risk mechanisms. In typhoon–rainfall–flood (TRF)-dominated regions, strengthening watershed-scale flood control infrastructure and protecting or restoring natural retention and detention spaces should be prioritized (Mitu et al., 2023; Rahim et al., 2024). In TRL-prone regions, where vulnerable populations account for a high proportion of residents (92.1 %), disaster risk reduction should extend beyond engineering measures to address social vulnerability. Key actions include community-based early warning and evacuation systems, registries of vulnerable groups, deployment of simple monitoring devices, and targeted slope stabilization and housing safety improvements (Zhuang et al., 2023; Zhao et al., 2024; Sarah et al., 2025).

5. Conclusion

Using Fujian Province as a case study, this research integrates a Copula-based joint probability model with explainable machine learning to systematically examine the spatial risk patterns, exposure inequality, and driving and transition mechanisms of typhoon disaster chains. The main findings are as follows: (1) High-risk areas of typhoon disaster chains in Fujian Province consist of both single disaster chains (SDCs) and compound disaster chains (CDCs), with eight typical disaster chain types identified. The mean joint occurrence probability of CDCs is 0.0082, which is 13.6 times higher than that of SDCs. Spatially, CDC high-risk areas are strongly clustered in major coastal cities, including Fuzhou, Xiamen, and Quanzhou, as well as in bay–estuary–urban transition zones. (2) Clear disparities in risk exposure exist between SDCs and CDCs. Although CDC high-risk areas account for only 0.8 % of the provincial area, they contain 12.6 % of the population and 14.1 % of the GDP, with population and GDP exposure lift values of 16.3 and 18.2, respectively. TRU (Typhoon–Rainfall–Urban Waterlogging)-related compound disaster chains exhibit a pronounced small-area, high-exposure pattern, whereas TRL (Typhoon–Rainfall–Landslide) high-risk areas show relatively low population density but an extremely high proportion of vulnerable populations (92.1 %). (3) Typhoon disaster chain risks generally follow a natural triggering–social amplification mechanism, in which natural hazard factors define the environmental background for hazard initiation, while social factors—particularly population density and GDP density—dominate risk amplification. Key driving variables exhibit clear nonlinear threshold behavior, such as a built-up area threshold of approximately 118,212 m^2/km^2 for TRF and an impervious surface ratio

threshold of 47 %–70 % for TRU-related compound disaster chains. (4) Transitions from single to compound disaster chains are governed by two dominant mechanisms: socioeconomic-driven pathways, mainly associated with TRU-related compound disaster chains, and naturally driven pathways, mainly associated with TRL- and TWS-related compound disaster chains. Population density plays a key role in the TRF → TRU + TRF transition, whereas persistent heavy rainfall dominates the TRF → TRF + TRL transition.

Several limitations should be noted. First, the analysis relies mainly on historical observations and relatively static socioeconomic indicators, which constrains its ability to represent cascading processes and temporal lag effects in disaster-chain evolution. Second, Fujian Province is characterized by mountainous coastal terrain and rapid urbanization, which may limit the direct extended applicability of some results to other regions. Identified threshold values therefore require further validation under different geographical and developmental contexts. In addition, the lack of high-resolution infrastructure data, such as urban drainage networks and coastal defense structures, may affect the detailed characterization of local compound flooding risks. Future research should address these limitations by incorporating time-dependent Copula models, process-based simulations, and cross-regional comparative analyses, thereby enhancing the dynamic representation, transferability, and explanatory depth of disaster chain risk assessment frameworks.

Beyond the specific case of Fujian Province, the proposed regional-scale analytical framework provides an adaptable approach for identifying compound disaster chain high-risk areas, exposure inequality patterns, and critical transition conditions. The framework offers practical support for managing compound flood and storm surge risks in highly urbanized coastal regions and can be extended to other multi-hazard areas influenced by climate change and rapid urbanization. More broadly, this study contributes to a shift in disaster risk research from single-hazard assessment toward integrated multi-hazard and socio–natural system analysis, with implications for hydrology, disaster geography, and integrated risk management.

CRediT authorship contribution statement

Laiyin Zhu: Software, Methodology. **Ying Chen:** Software, Methodology. **Jiewen You:** Software, Methodology. **Miaomiao Ma:** Software, Data curation. **Xiaochen Qin:** Software, Methodology. **Xiaoliu Yang:** Writing – original draft, Software, Methodology, Formal analysis, Data curation. **Harald Kunstmann:** Software, Methodology. **Lu Gao:** Writing – review & editing, Supervision, Resources, Investigation, Conceptualization. **Jianhui Wei:** Software, Methodology.

Declaration of Competing Interest

The authors declare that they have no known competing financial interests or personal relationships that could have appeared to influence the work reported in this paper.

Acknowledgements

This work was funded by the National Natural Science Foundation of China (Grant No. 42271030), the "Young Eagle Plan" Top Talents of Fujian Province, and the Federal Ministry of Education and Research (BMBF) through the KARE II project (Grant No. 01LR2006D1). Jianhui Wei is financially supported by the Federal Ministry of Research, Technology and Space through funding of the KAR II project (01LR2006D1). Lu Gao is financially supported by the Humboldt Research Fellowship for Experienced Researchers through Alexander von Humboldt Foundation.

Data availability

Data will be made available on request.

References

Aas, K., Czado, C., Frigessi, A., Bakken, H., 2009. Pair-copula constructions of multiple dependence. Insur. Math. Econ. 44 (2), 182–198.
AghaKouchak, A., Huning, L., Chiang, F., Sadegh, M., Vahedifard, F., Mazdiyasni, O., Moftakhari, H., Mallakpour, I., 2018. How do natural hazards cascade to cause disasters? Nature 561, 458–460.
Alfieri, L., Dottori, F., Salamon, P., Wu, H., Feyen, L., 2020. Global modeling of seasonal mortality rates from river floods. Earths Future 8, e2020EF001541.
Bates, P.D., Quinn, N., Sampson, C., Smith, A., Wing, O., Sosa, J., Savage, J., Olcese, G., et al., 2021. Combined modeling of US fluvial, pluvial, and coastal flood hazard under current and future climates. Water Resour. Res. 57, 1–29.
Bevacqua, E., Vousdoukas, M., Zappa, G., Hodges, K., Shepherd, T., Maraun, D., Mentaschi, L., Feyen, L., 2020. More meteorological events that drive compound coastal flooding are projected under climate change. Commun. Earth Environ. 1, 47.
Cai, L., Li, Y., Chen, M., Zou, Z., 2020. Tropical cyclone risk assessment for China at the provincial level based on clustering analysis. Geomat. Nat. Hazards Risk. 11 (1), 869–886.
Chen, A., Pokhrel, Y., Chen, D., Huang, H., Dai, Z., He, B., Wang, J., Li, J., et al., 2024. Impact of tropical cyclones and socioeconomic exposure on flood risk distribution in the Mekong Basin. Commun. Earth Environ. 5, 704.
Chen, X., Wang, J.A., Chen, J., 2007. Primary study on spatiotemporal change and regional lization of storm-flood in Fujian Province. J. Nat. Disasters 16, 1–7 (in Chinese).
Cramer, W., Guiot, J., Fader, M., Garrabou, J., Gattuso, J., Iglesias, A., Lange, M., Lionello, P., et al., 2018. Climate change and interconnected risks to sustainable development in the Mediterranean. Nat. Clim. Change 8, 972–980.
Cutter, S.L., Barnes, L., Berry, M., Burton, C., Evans, E., Tate, E., Webb, J., 2008. A place-based model for understanding community resilience to natural disasters. Glob. Environ. Change 18, 598–606.
Dawit, G.B., Shankar, K., Gemachu, S., 2023. Identifying flood vulnerable and risk areas using the integration of analytical hierarchy process (AHP), GIS, and remote sensing: A case study of southern Oromia region. Urban Clim. 51, 101640.

Deb, M., Sun, N., Yang, Z., Wang, T., Judi, D., Xiao, Z., Wigmosta, M.S., 2023. Interacting effects of watershed and coastal processes on the evolution of compound flooding during Hurricane Irene. Earth's. Future 11, e2022EF002947.
Dey, H., Haque, M., Shao, W., VanDyke, M., Hao, F., 2024. Simulating flood risk in Tampa Bay using a machine learning driven approach. npj Nat. Hazards 1, 40.
Dey, H., Shao, W., Haque, M.M., VanDyke, M., 2024. Enhancing flood risk analysis in Harris County: integrating flood susceptibility and social vulnerability mapping. J. Geovisualization Spat. Anal. 8, 19.
Do, C., Kuleshov, Y., 2023. Multi-hazard tropical cyclone risk assessment for Australia. Remote Sens 15, 795.
Dottori, F., Szewczyk, W., Ciscar, J.C., Zhao, F., 2022. Increased human and economic losses from river flooding with anthropogenic warming. Nat. Clim. Change 8, 781–786.
Feng, K., Ouyan, M., Lin, N., 2022. Tropical cyclone-blackout-heatwave compound hazard resilience in a changing climate. Nat. Commun. 13, 4421.
Feng, D., Tan, Z., Xu, D., Ruby Leung, L., 2023. Understanding the compound flood risk along the coast of the contiguous United States. Hydrol. Earth Syst. Sci. 27, 3911–3934.
Frahm, G., Junker, M., Schmidt, R., 2005. Estimating the tail-dependence coefficient: Properties and pitfalls. Insur. Math. Econ. 37 (1), 80–100.
Ganguli, P., Lin, N., 2025. Intense humid heat — tropical cyclone compound hazards in eastern coastal India. npj Nat. Hazards 2, 49.
Ganguli, P., Merz, B., 2024. Observational evidence reveals compound humid heat stress-extreme rainfall hotspots in India. Earths Future 12, e2023EF004074.
Gori, A., Lin, N., Xi, D., 2020. Tropical cyclone compound flood hazard assessment: from investigating drivers to quantifying extreme water levels. Earths Future 8 (12), 6 e2020EF001660.
Gori, A., Lin, N., Xi, D., Emanuel, K., 2022. Tropical cyclone climatology change greatly exacerbates US extreme rainfall–surge hazard. Nat. Clim. Change 12, 171–178.
Grimley, L., Hollinger Beatty, K., Sebastian, A., Bunya, S., Lackmann, G., 2024. Clim. Change exacerbates Compd. flooding Recent Trop. Cyclones npj Nat. Hazards 2024 (1), 45.
Hallegatte, S., Green, C., Nicholls, R.J., Corfee-Morlot, J., 2013. Future flood losses in major coastal cities. Nat. Clim. Change 3, 802–806.
Han, P., Guo, G.Z., Li, X.L., Liu, Q.Q., 2023. Research on influencing factors of typhoon disasters in Fujian Province based on geodetector. Remote Sens. Technol. Appl. 38, 487–495 (in Chinese).
Haque, M.M., Islam, S., Sikder, M.B., Islam, M.S., 2022. Community flood resilience assessment in Jamuna floodplain: a case study in Jamalpur District Bangladesh. Int. J. Disaster Risk Reduct. 72, 102861.
Hoque, M.A., Phinn, S., Roelfsema, C., Childs, I., 2018. Assessing tropical cyclone risks using geospatial techniques. Appl. Geogr. 98, 22–33.
Javed, A., Thomas, W., Joao, M., Alejandra, E., Melanie, G., Christopher, E., 2025. Multivariate compound events drive historical floods and associated losses along the U.S. East and Gulf coasts. npj Nat. Hazards 2, 19.
Jiang, R., Heft-Neal, S., Chavas, D., Griswold, M., Wang, Z., Clark-Ginsberg, A., Guha-Sapir, D., Bendavid, E., Wagner, Z., 2023. Global population profile of tropical cyclone exposure from 2002 to 2019. Nature 626, 15.
Jiang, H., Zipser, E.J., 2010. Contribution of tropical cyclones to the global precipitation from eight seasons of TRMM data: Regional, seasonal, and interannual variations. J. Clim. 23, 1526–1543.
Lai, Y., Li, J., Gu, X., Wu, G., 2020. Greater flood risks in response to slowdown of tropical cyclones over the coast of China. Proc. Natl. Acad. Sci. 117, 14751–14755.
Li, C., Liu, M., Hu, Y., Wang, H., Zhou, R., Wu, W., Wang, Y., 2022. Spatial distribution patterns and potential exposure risks of urban floods in Chinese megacities. J. Hydrol. 610, 127838.
Li, Y., Zhou, W., Shen, P., 2023. Flood risk assessment of loss of life for a coastal city under the compound effect of storm surge and rainfall. Urban Clim. 47, 101396.
Liang, X., Segoni, S., Yin, K., Du, J., Chai, B., Tofani, V., Casagli, N., 2022. Characteristics of landslides and debris flows triggered by extreme rainfall in Daoshi Town during the 2019 Typhoon Lekima, Zhejiang Province, China. Landslides 19, 1735–1749.
Liang, Y., Wang, C., Chen, G., Xie, Z., 2024. Evaluation framework ACR-UFDR for urban form disaster resilience under rainstorm and flood scenarios: a case study in Nanjing, China. Sustain. Cities Soc. 107, 105424.
Lin, N., Emanuel, K., Oppenheimer, M., Vanmarcke, E., 2012. Physically based assessment of hurricane surge threat under climate change. Nat. Clim. Change 2, 462–467.
Liu, F., Xu, E., Zhang, H., 2022. An improved typhoon risk model coupled with mitigation capacity and its relationship to disaster losses. J. Clean. Prod. 357, 131913.
Lockwood, J.W., Lin, N., Gori, A., Oppenheimer, M., 2024. Increasing flood hazard posed by tropical cyclone rapid intensification in a changing climate. Geophys. Res. Lett. 51, e2023GL105624.
Malakar, K., Mishra, T., Hari, V., Karmakar, S., 2021. Risk mapping of Indian coastal districts using IPCC-AR5 framework and multi-attribute decision-making approach. J. Environ. Manag. 294, 112948.
Mantovani, J., Alcântara, E., Pampuch, L., Baião, C.F.P., Park, E., Custódio, M.S., Gozzo, L.F., Bortolozo, C.A., 2024. Assessing flood risks in the Taquari-Antas Basin (Southeast Brazil) during the September 2023 extreme rainfall surge. npj Nat. Hazards 1, 9.
Marsooli, R., Lin, N., Emanuel, K., Feng, K., 2019. Climate change exacerbates hurricane flood hazards along US Atlantic and Gulf Coasts in spatially varying patterns. Nat. Commun. 10, 1–9.
Mazdiyasni, O., AghaKouchak, A., 2015. Substantial increase in concurrent droughts and heatwaves in the United States. Proc. Natl. Acad. Sci. 112, 11484–11489.
McMichael, C., Dasgupta, S., Ayeb-Karlsson, S., Kelman, L., 2020. A review of estimating population exposure to sea-level rise and the relevance for migration. Environ. Res. Lett. 15 (12), 123005.
Meng, S., Wang, W., Zhang, K., 2025. Beyond wind and rainfall: insights into Hurricane Helene fatalities with the National Risk Index. npj Nat. Hazards 2, 38.
Messori, G., Bevacqua, E., Caballero, R., Coumou, D., Luca, P., Faranda, D., Kornhuber, K., Martius, O., et al., 2021. Compound climate events and extremes in the midlatitudes: dynamics, simulation, and statistical characterization. Bull. Am. Meteorol. Soc. 102. E774-E781.
Mitsova, D., Esnard, A.M., Sapat, A., Lai, B.S., 2018. Socioeconomic vulnerability and electric power restoration timelines in Florida: the case of Hurricane Irma. Nat. Hazards 94, 689–709, 5.
Mitu, M., Sofia, G., Shen, X., Anagnostou, E., 2023. Assessing the compound flood risk in coastal areas: Framework formulation and demonstration. J. Hydrol. 626, 130278.
Moftakhari, H.R., Salvadori, G., AghaKouchak, A., Sanders, B.F., Matthew, R.A., 2017. Compounding effects of sea level rise and fluvial flooding. Proc. Natl. Acad. Sci. 114, 9785–9790.
Mohtat, N., Khirfan, L., 2022. Distributive justice and urban form adaptation to flooding risks: Spatial Analysis to identify Toronto's priority neighborhoods. Front. Sustain. Cities 4.
Morita, T., Nomura, S., Tsubokura, M., Leppold, C., Gilmour, S., Ochi, Sae, Ozaki, A., Shimada, Y., et al., 2017. Excess mortality due to indirect health effects of the 2011 triple disaster in Fukushima, Japan: a retrospective observational study. J. Epidemiol. Community Health 71, 974–980.
Naseri, K., Hummel, M.A., 2022. A Bayesian copula-based nonstationary framework for compound flood risk assessment along US coastlines. J. Hydrol. 610, 128005.
Otto, C., Piontek, F., Kalkuhl, M., Frieler, K., 2020. Event-based models to understand the scale of the impact of extremes. Nat. Energy 5, 111–114.
Peduzzi, P., Chatenoux, B., Dao, H., Bono, A., Herold, C., Kossin, J., Mouton, F., Nordbeck, O., 2012. Global trends in tropical cyclone risk. Nat. Clim. Change 12, 289–294.
Peduzzi, P., Dao, H., Herold, C., Mouton, F., 2009. Assessing global exposure and vulnerability towards natural hazards: the Disaster Risk Index. Nat. Hazards Earth Syst. Sci. 9, 1149–1159.
Peng, Z., Mo, S., Sun, A.Y., Wu, J., Zeng, X., Lu, M., Shi, X., 2025. An explainable Bayesian TimesNet for probabilistic groundwater level prediction. Water Resour. Res. 61, e2025WR040191.
Qiao, R., Gao, S., Liu, X., Xia, L., Zhang, G., Meng, X., Liu, Z., Wang, M., Zhou, S., Wu, Z., 2024. Understanding the global subnational migration patterns driven by hydrological intrusion exposure. Nat. Commun. 15, 6285.
Rahim, M., Assi, A., Mostafiz, R., Friedland, C., 2024. Effects of damage initiation points of depth-damage function on flood risk assessment. npj Nat. Hazards 1, 6.
Ranjan, R., Karmakar, S., 2024. Compound hazard mapping for tropical cyclone-induced concurrent wind and rainfall extremes over India. npj Nat. Hazards 1, 15.

Ravi, R., Subhankar, K., 2024. Compound hazard mapping for tropical cyclone-induced concurrent wind and rainfall extremes over India. npj Nat. Hazards 1, 15.
Raymond, C., Matthews, T., Horton, R.M., 2020. The emergence of heat and humidity too severe for human tolerance. Sci. Adv. 6, eaaw1838.
Sarah, S., Zebedee, N., Roman, H., Setu, P., Carl-Friedrich, S., 2025. High-income groups disproportionately contribute to climate extremes worldwide. Nat. Clim. Change 15, 627–633.
Tang, P., Zhong, W., Wen, J., Shao, S., Zhou, D., 2023. Developing and understanding cascading effects scenario of typhoons in coastal mega-cities from system perspectives for disaster risk reduction. Int. J. Disaster Risk Reduct. 93, 103781.
Tran, T.L., Ritchie, E., Perkins-Kirkpatrick, S., Bui, H., Luong, T., 2022. Future changes in tropical cyclone exposure and impacts in Southeast Asia from CMIP6 pseudo-global warming simulations. Earths Future 10 (12), e2022EF003118.
Tu, Y., Shi, H., Chen, K., Liang, Y., Zhou, X., Lev, B., 2022. Three-reference-point based group ELECTRE III method for urban flood resilience evaluation. Expert Syst. Appl. 210, 118488.
Turner, B.L., Kasperson, R.E., Matson, P., McCarthy, J., Corell, R., Christensen, L., Eckley, N., Kasperson, J., et al., 2003. A framework for vulnerability analysis in sustainability science. Proc. Natl. Acad. Sci. USA 100, 8074–8079.
VanDyke, M.S., Armstrong, C.L., Bareford, K., 2021. How risk decisionmakers interpret and use flood forecast information: assessing the Mississippi River Outlook email product. J. Risk Res. 24, 1239–1250.
Wahl, T., Jain, S., Bender, J., Meyers, S.D., Luther, M.E., 2015. Increasing risk of compound flooding from storm surge and rainfall for major US cities. Nat. Clim. Chang. 5, 1093–1097.
Wang, Z., Nan, X., Zhao, X., Ji, X.K., Wang, J.C., 2024. Comprehensive risk assessment of typhoon disasters in China's coastal areas based on multi-source geographic big data. Sci. Total Environ. 926, 171815 (Article).
Wang, Y., Peng, L., Yang, L.E., Wang, Z., Deng, X., 2024. Attributing effects of classified infrastructure management on mitigating urban flood risks: a case study in Beijing, China. Sustain. Cities Soc. 101, 105141.
Xi, D., Lin, N., Gori, A., 2023. Increasing sequential tropical cyclone hazards along the US East and Gulf coasts. Nat. Clim. Chang. 13 (3), 258–265.
Yang, X., Qin, X., Zhou, X., Chen, Y., Gao, L., 2024. Assessment of disaster mitigation capability oriented to typhoon disaster chains: A case study of Fujian Province, China. Ecol. Indic. 167, 112621.
Yang, X., Yan, Y., Zhou, L., Ma, M., Zhang, J., Chen, Y., Gao, L., 2025. Risk of Compound Typhoon Disaster Chains: Insights from Southeastern China. Int. J. Disaster Risk Sci. 16, 870–887.
Yang, M., Yusoff, W.F.M., Mohamed, M.F., Jiao, S., Dai, Y., 2024. Flood economic vulnerability and risk assessment at the urban mesoscale based on land use: A case study in Changsha, China. J. Environ. Manag. 351, 119798.
Ye, P., Yu, B., Chen, W.H., Liu, K., Ye, L.Z., 2022. Rainfall-induced landslide susceptibility mapping using machine learning algorithms and comparison of their performance in Hilly area of Fujian Province, China. Nat. Hazards 113, 965–995.
Young, R., Hsiang, S., 2024. Mortality caused by tropical cyclones in the United. S. Nat. 635, 7.
Yu, S., Kong, X., Wang, Q., Yang, Z., Peng, J., 2023. A new approach of Robustness-Resistance-Recovery (3Rs) to assessing flood resilience: a case study in Dongting Lake Basin. Landsc. Urban Plan. 230, 104605.
Zhang, J., Chen, Y., 2019. Risk assessment of flood disaster induced by typhoon rainstorms in Guangdong Province, China. Sustainability 11, 2738.
Zhang, Q., Li, C., Wen, D., Kang, J., Chen, T., Zhang, B., Hu, Y., Yin, J., Slater, L., 2025. Global South shows higher urban flood exposures than the Global North under current and future scenarios. Commun. Earth Environ. 6, 594.
Zhao, Q., Gao, L., Meng, Q., Zhu, M., 2024. Climate warming will exacerbate unequal exposure to compound flood-heatwave extremes. Earths Future 12, e2024EF005179.
Zhu, S., Li, D., Feng, H., Zhang, N., 2023. The influencing factors and mechanisms for urban flood resilience in China: From the perspective of social-economic-natural complex ecosystem. Ecol. Indic. 147, 109959.
Zhuang, Y., Xing, A., Sun, Q., Jiang, Y., Zhang, Y., Wang, C., 2023. Failure and disaster-causing mechanism of a typhoon-induced large landslide in Yongjia, Zhejiang, China. Landslides 20, 2257–2269.
Zscheischler, J., Martius, O., Westra, S., Bevacqua, E., Raymond, C., Horton, R., Hurk, B., Aghakouchak, A., et al., 2020. A typology of compound weather and climate events. Nat. Rev. Earth Environ. 1, 333–347.
Zscheischler, J., Westra, S., Hurk, S., Seneviratne, S., Ward, P., Pitman, A., Aghakouchak, A., Bresch, D., et al., 2018. Future climate risk from compound events. Nat. Clim. Change 8, 469–477.